

Modeling and Controls of Fluid-Structure Interactions (FSI) in Dynamic Morphing Flight

Bibek Gupta¹, Eric Sihite² and Alireza Ramezani^{1*}

Abstract—The primary aim of this study is to enhance the accuracy of our aerodynamic Fluid-Structure Interaction (FSI) model to support the controlled tracking of 3D flight trajectories by Aerobat, which is a dynamic morphing winged drone. Building upon our previously documented Unsteady Aerodynamic model rooted in horseshoe vortices, we introduce a new iteration of Aerobat, labeled as version β , which is designed for attachment to a Kinova arm. Through a series of experiments, we gather force-moment data from the robotic arm attachment and utilize it to fine-tune our unsteady model for banking turn maneuvers. Subsequently, we employ the tuned FSI model alongside a collocation control strategy to accomplish 3D banking turns of Aerobat within simulation environments. The primary contribution lies in presenting a methodical approach to calibrate our FSI model to predict complex 3D maneuvers and successfully assessing the model’s potential for closed-loop flight control of Aerobat using an optimization-based collocation method.

I. INTRODUCTION

Dynamic morphing winged systems, akin to bats or birds, dexterously manipulate their fluidic environment [1]. This ability to modulate fluid momentum through controlled movements in three dimensions distinguishes vertebrate flight from that of insects [2] and is key to vertebrates’ agile and efficient flight.

Research on drones with adaptive body structures similar to bats and birds has been ongoing for many years [3]. These systems often possess slow moving joints that do not match dynamic morphing capabilities seen in vertebrate fliers. For instance, bats are able to move over forty joints dynamically during one gait cycle [4].

The emergence of small form factor electronics and actuators has enabled the development of new small robots capable of dynamically adjusting their body configurations dynamically [5]–[8]. The Northeastern University Aerobat [9]–[16] aims to perfect controlled fluidic manipulations. This robot has an articulated wing structure as is able to dynamically move its joints during one wingcycle, about one tenth of a second.

Dynamic morphing of wings introduces complex fluid-structure interactions, rendering existing quasi-steady models used in insect flight inadequate [17]. Moreover, these morphing wing robots feature heavier wings that deviate from the two-time scale dynamical models typically applied to

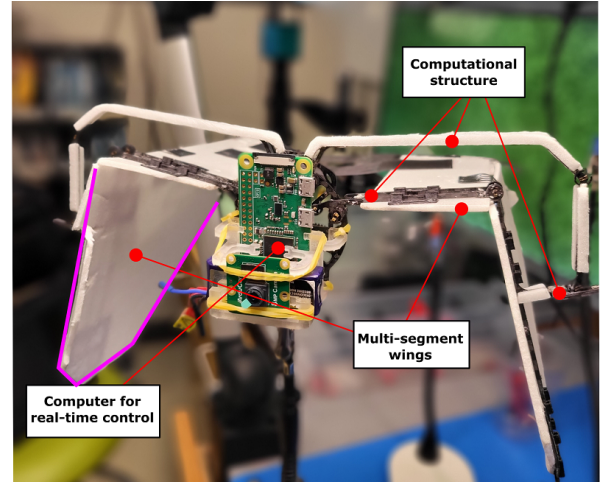


Fig. 1. Shows Northeastern University Aerobat platform designed to inspect dynamic morphing wing flight

insects [18]. Consequently, these systems not only present distinctive opportunities for hardware design but also offer rich prospects for modeling and control.

In our previous studies, we introduced unsteady fluid-structure models predicting the force-moment profile in Aerobat flight [10] motivated by prior works such as [19] and [20]. This model accommodated the step response of the lift coefficient as the morphing wing undergoes plunge movements and flexion-extensions in the armwings.

We experimentally validated this model’s accuracy for hovering maneuvers by subjecting Aerobat to varying upstream flow conditions [21]. Based on these results, we applied this model to design a hovering controller in a tandem configuration in [21]. The unsteady model, coupled with an extended state observer (ESO), estimated FSI in the tandem structure, which was then used to control the tandem platform.

In this study, our overarching objective is to expand Aerobat’s flight capabilities beyond hovering, encompassing banking turns, sharp dives, heel-above-the-head landings, and more. These locomotive maneuvers demand enhanced accuracy of the unsteady model as Aerobat traverses complex 3D paths. The main contributions of this publication are: i) the presentation of the test platform developed for tuning the unsteady model as Aerobat navigates complex 3D paths, ii) the collection and comparison of experimental data with the unsteady simulator, and iii) the utilization of the tuned model to design a collocation-based controller for tracking

¹Authors are with the Silicon Synapse Labs, Department of Electrical and Computer Engineering, Northeastern University, Boston, USA. Emails: gupta.bi, a.ramezani@northeastern.edu

²Author is with the Department of Aerospace Engineering, California Institute of Technology, Pasadena, USA. Email: esihite@caltech.edu

*Corresponding author.

a 3D path in simulation.

This work is organized as follows: we begin with the hardware and constrained model overview, followed by the summary of the unsteady aerodynamic model used to estimate the fluid-structure interactions (FSI), 3D path tracking and control. Then, it will be followed by the result discussions and concluding remarks.

II. CONSTRAINED MODEL HARDWARE OVERVIEW

To emulate 3D path flights and record FSI from experiments, we design a version of Aerobat, called version- β , and fixated the design to the end-effector of a Kinova arm as shown in Fig. 2. Aerobat- β , similar to other versions [10], possesses a computational structure [22] that generates dynamic coupled joint movements. The resulting wing movements include (1) plunge movements at the shoulders and (2) flexion-extension motions at the elbows. A gait generator, a brushless-dc motor with gearbox, drives the computational structure.

The Aerobat- β model hardware lacks orientation control, rendering it incapable of executing banking turns independently in untethered fashion. To overcome this limitation, for model turning purposes, this study utilizes a Gen-3 6-DOF Kinova robotic arm (see Fig. 2), characterized by its joint speed reaching up to 70 degrees per second and a linear end-effector speed capacity of up to 50 cm/s.

Next, as shown in Fig. 2, through the integration of the Aerobat robot onto the Kinova arm's end-effector via a custom-designed 3D printed mount equipped with an ATI load cell, we recorded force-moment profile during the execution of banking turns as shown in Fig. 3. This ATI load cell is a Nano17 6-axis-transducer model, having a Net box for data acquisition via Ethernet, and has rated capacities of 480 N for load force and 1.9 N·m for load torque. Using the load cell, data for both force and moments were collected at a sampling frequency of 7 kHz during the banking maneuver experiments.

III. UNSTEADY MODEL USED TO PREDICT FLUID-STRUCTURE INTERACTIONS (FSI)

The unsteady lift aerodynamic model derived in this section follows similar derivations to [19]. This model uses the lifting line theory and Wagner's function to develop a model for calculating the lift coefficient. Let S be the total wingspan and $y \in [-S/2, S/2]$ represents a position along the wingspan. The circulation distribution on the wing can be defined as a function of truncated Fourier series of size m across the wingspan, as follows:

$$\Gamma(t, y) = \frac{1}{2} a_0 c_0 U \sum_{n=1}^m a_n(t) \sin(n\theta(y)) \quad (1)$$

where a_n is the Fourier coefficients, a_0 is the slope of the angle of attack, c_0 is the chord length at wing's axis of symmetry, and U is the free stream airspeed. Then θ is the change of variable defined by $y = (S/2) \cos(\theta)$ for describing a position along the wingspan $y \in (-S/2, S/2)$.

From $\Gamma(t, y)$, we can derive the additional downwash induced by the vortices, defined as follows:

$$\begin{aligned} w_y(t, y) &= -\frac{1}{4\pi} \int_{-S/2}^{S/2} \frac{d\Gamma/dy_0}{y-y_0} dy_0 \\ &= -\frac{a_0 c_0 U}{4S} \sum_{n=1}^m n a_n(t) \frac{\sin(n\theta)}{\sin(\theta)}. \end{aligned} \quad (2)$$

Following the unsteady Kutta-Joukowski theorem, the sectional lift coefficient can be expressed as follows:

$$\begin{aligned} C_L(t, y) &= \frac{2\Gamma}{Uc(y)} + \frac{2\dot{\Gamma}}{U^2} \\ &= a_0 \sum_{n=1}^m \left(\frac{c_0}{c(y)} a_n(t) + \frac{c_0}{U} \dot{a}_n(t) \right) \sin(n\theta), \end{aligned} \quad (3)$$

where $c(y)$ is the chord length at the wingspan position y . The computation of the sectional lift coefficient response of an airfoil undergoing a step change in downwash $\Delta w(y) \ll U$ can be expressed using Wagner function $\Phi(\tilde{t})$:

$$\begin{aligned} c_L(t, y) &= \frac{a_0}{U} \Delta w(t, y) \Phi(\tilde{t}) \\ \Phi(\tilde{t}) &= 1 - \psi_1 e^{-\varepsilon_1 \tilde{t}} - \psi_2 e^{-\varepsilon_2 \tilde{t}} \end{aligned} \quad (4)$$

where $\tilde{t}(t) = \int_0^t (v_e^i/b) dt$ is the normalized time which is defined as the distance traveled divided by half chord length ($b = c/2$). Here, v_e^i is defined as the velocity of the quarter chord distance from the leading edge in the direction perpendicular to the wing sweep. For the condition where the freestream airflow dominates v_e , then we can approximate the normalized time as $\tilde{t} = Ut/b$. The Wagner model in (4) uses Jones' approximation [19], with the following coefficients: $\psi_1 = 0.165$, $\psi_2 = 0.335$, $\varepsilon_1 = 0.0455$, and $\varepsilon_2 = 0.3$.

IV. 3D PATH TRACKING AND CONTROLS

To solve this flight control problem, i.e., Aerobat's posture y_1 is recruited to regulate fluid-structure forces-moments y_2 to track a 3D path, we consider the following cost function given by

$$J = \sum_i^N (z_i - z_{ref,i})^\top C (z_i - z_{ref,i}), \quad z = [\theta_r, \theta_p, \omega^\top]^\top, \quad (5)$$

where θ_r and θ_p represent the robot's roll and pitch angles relative to the inertial frame, respectively, while ω represents the robot's angular velocities, z is the optimization state, z_{ref} is the state reference for z , and C is a diagonal cost weighting matrix. The cost function J is governed by a system of n nonlinear equations representing the computational structure dynamics driven by low-power actuators.

To further elucidate, following the principle of virtual work [23], the response from the computational structure can

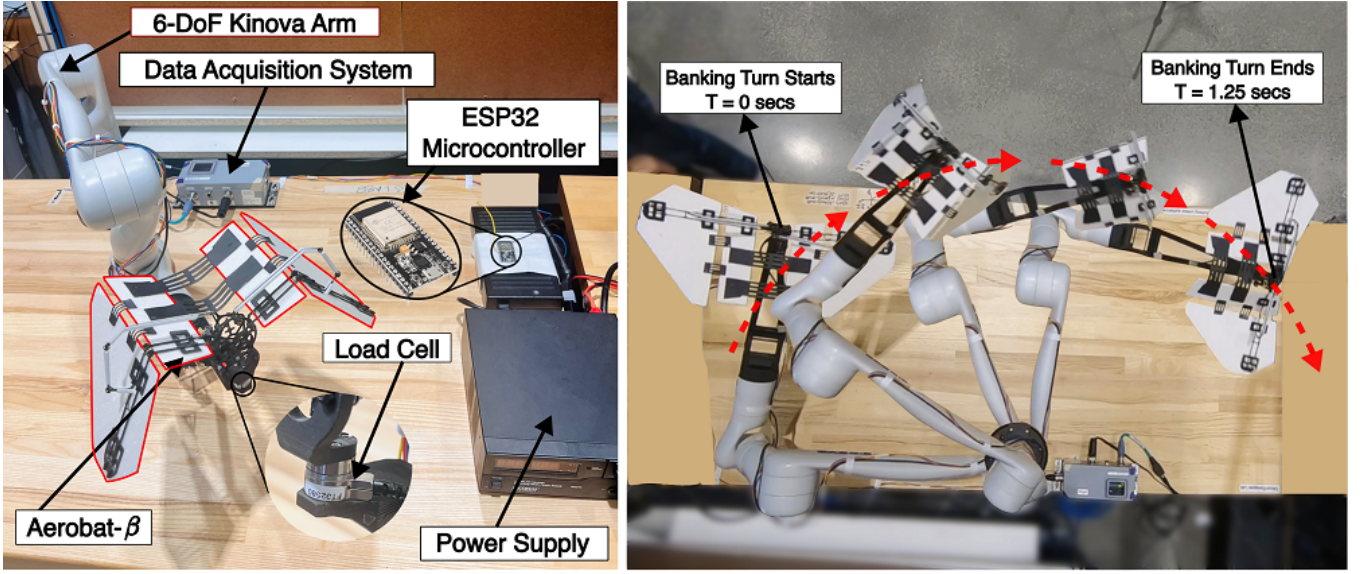


Fig. 2. (a) Shows the test setup, including the arm, load-cell, Aerobat version β , and data acquisition system. (b) Snapshots of arm and Aerobat during the constrained banking turn at different sample times are overlaid and illustrated in this image.

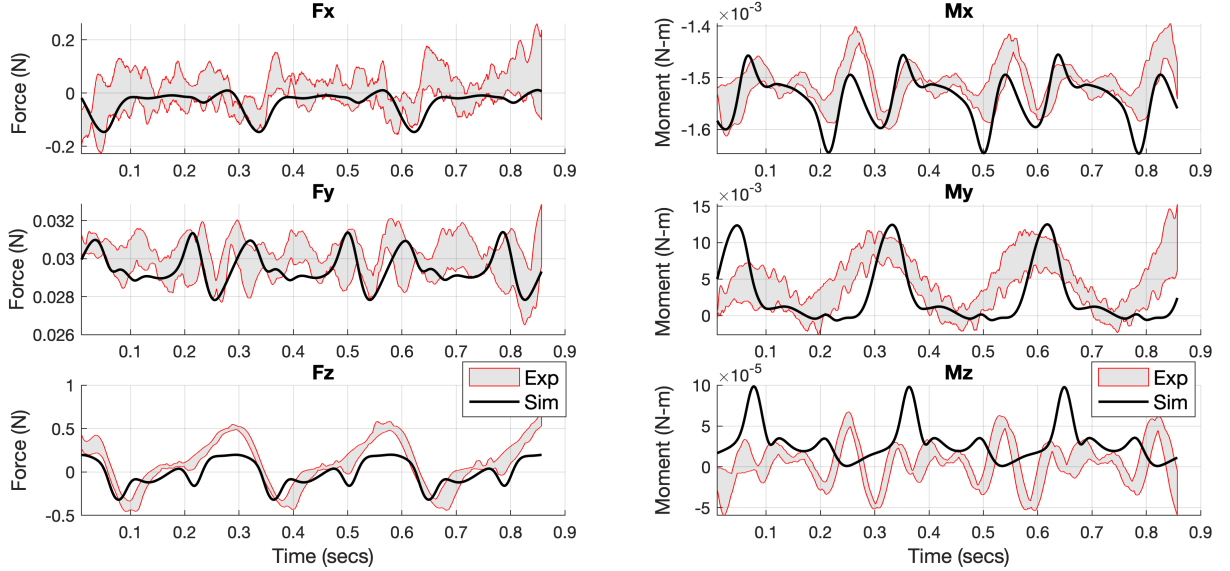


Fig. 3. Illustrates comparison of the force-moment trajectories between experiment and simulation.

be determined by

$$\begin{bmatrix} \dot{y}_{1,1} \\ \ddot{y}_{1,1} \\ \vdots \\ \dot{y}_{1,n} \\ \ddot{y}_{1,n} \end{bmatrix} = \begin{bmatrix} a_{1,1} & a_{1,2} & \dots \\ \vdots & \ddots & \\ a_{2n,1} & & a_{2n,2n} \end{bmatrix} \begin{bmatrix} y_{1,1} \\ \dot{y}_{1,1} \\ \vdots \\ y_{1,n} \\ \dot{y}_{1,n} \end{bmatrix} + \begin{bmatrix} b_{1,1} & b_{1,2} & \dots \\ \vdots & \ddots & \\ b_{2n,1} & & b_{2n,m} \end{bmatrix} \begin{bmatrix} \omega_1 \\ \vdots \\ \omega_m \end{bmatrix} \quad (6)$$

where $y_{1,j}$, $j = 1, \dots, n$ denotes the movement from each element of the computational structure, $a_{j,k}$ and $b_{j,k}$ are determined by the physical properties, and ω_j , $j = 1, \dots, m$

is the regulator's input.

By inspecting Eq. 6, it can be observed that the contribution of the input term u based on mode generation and regulation can be separately considered through the design of $a_{j,k}$ (i.e., structure configuration and material properties) and $b_{j,k}$ (regulator or low-power actuator placement), as discussed in [24].

We perform temporal (i.e., t_i , $i = 1, \dots, n$, $0 \leq t_i \leq t_f$) discretization of Eq. 6 to obtain the following system of equations

$$\dot{Y}_i(t_i) = A_i Y_i(t_i) + B_i \Omega_i(t_i), \quad i = 1, \dots, n, \quad 0 \leq t_i \leq t_f \quad (7)$$

where $Y_i = [y_{1,1}^\top, \dots, y_{1,n}^\top]^\top$ embodies n spatial values of the computational structure response at i -th discrete time

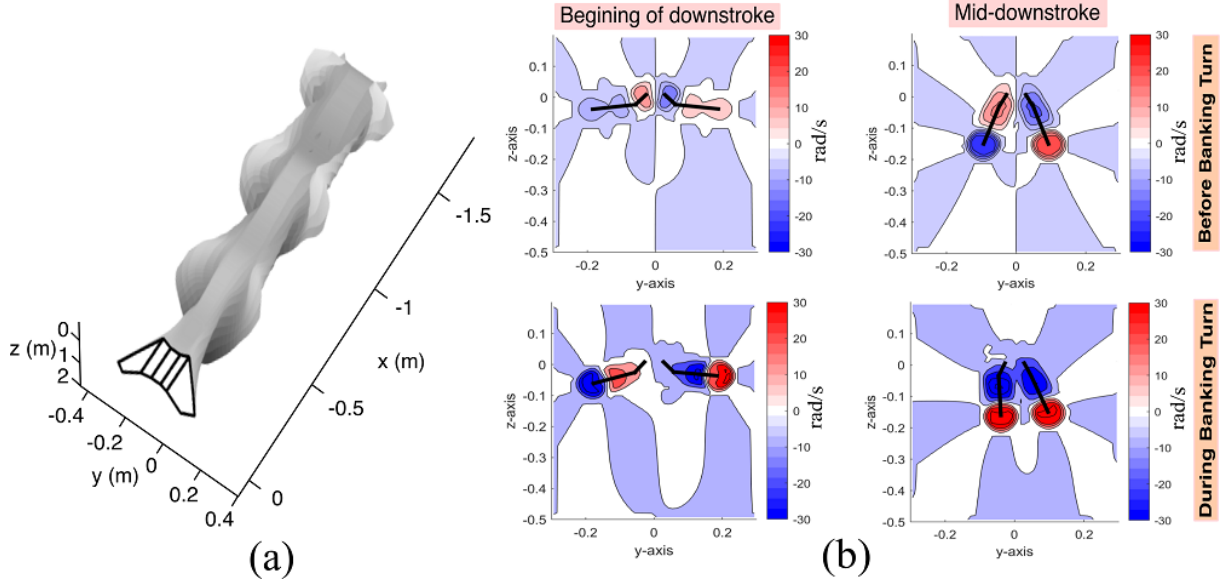


Fig. 4. Illustrates wake structures (iso-metric view) and vorticity plots in the frontal plane of flapping at (i) the beginning of downstroke, (ii) middle of downstroke, (iii) beginning of upstroke, and (iv) the middle of upstroke during banking turn.

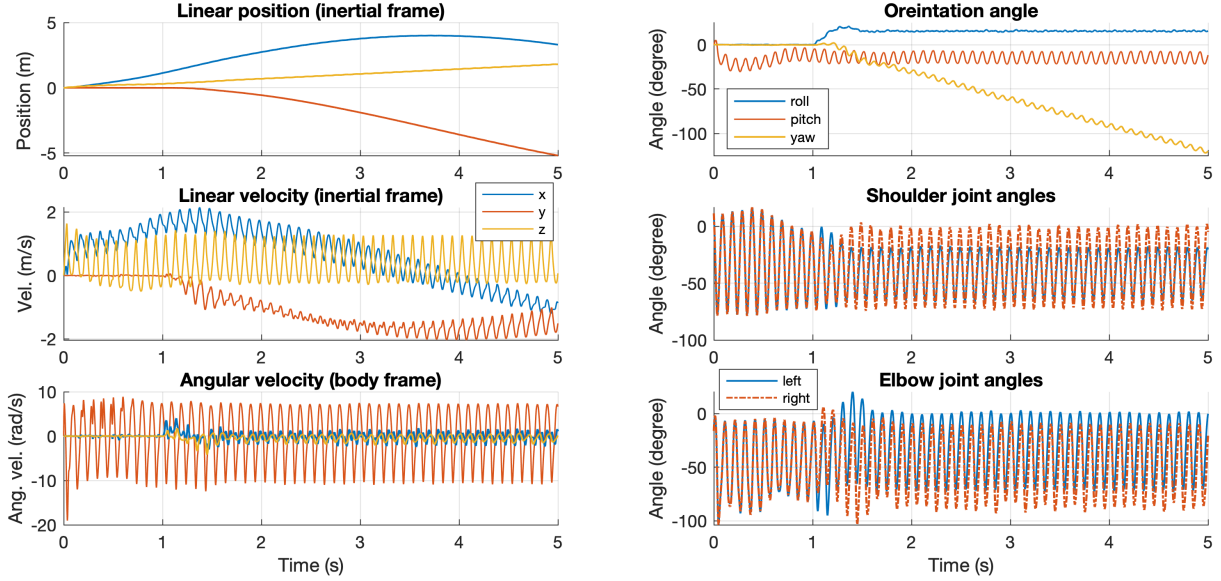


Fig. 5. Shows all of Aerobat state trajectories including body orientation, position, and body angles (shoulder and elbow joints).

(i.e., posture at time t_i). And, $\Omega_i = [\omega_1, \dots, \omega_m]$ embodies m regulators actions at i -th discrete time. A_i and B_i are the matrices shown in Eq. 6 with their entries.

We stack all of the postures and low-power inputs from the regulators from each i -th sample time, i.e., Y_i and Ω_i , in the vectors $Y = [Y_1^\top(t_1), \dots, Y_n^\top(t_n)]^\top$ and $\Omega = [\Omega_1^\top(t_1), \dots, \Omega_m^\top(t_n)]^\top$.

We consider $2n$ boundary conditions at the boundaries of n structure elements (2 equations at each boundary) to enforce the continuity of the computational structure, given by

$$r_i(Y(0), Y(t_f), t_f) = 0, \quad i = 1, \dots, 2n \quad (8)$$

Since we have m regulators, we consider m inequality

constraints given by

$$g_i(Y(t_i), \Omega(t_i), t_i) \geq 0, \quad i = 1, \dots, m, \quad 0 \leq t_i \leq t_f \quad (9)$$

to limit the actuation stroke from the low-power actuators.

To approximate nonlinear dynamics from the computational structure, we employ a method based on polynomial interpolations. This method extremely simplifies the computation efforts. Consider the n time intervals during a gait cycle of the dynamic morphing system, as defined previously and given by

$$0 = t_1 < t_2 < \dots < t_n = t_f \quad (10)$$

We stack the states and regulator inputs $Y = [Y_1^\top(t_1), \dots, Y_n^\top(t_n)]^\top$ and $\Omega = [\Omega_1^\top(t_1), \dots, \Omega_m^\top(t_n)]^\top$

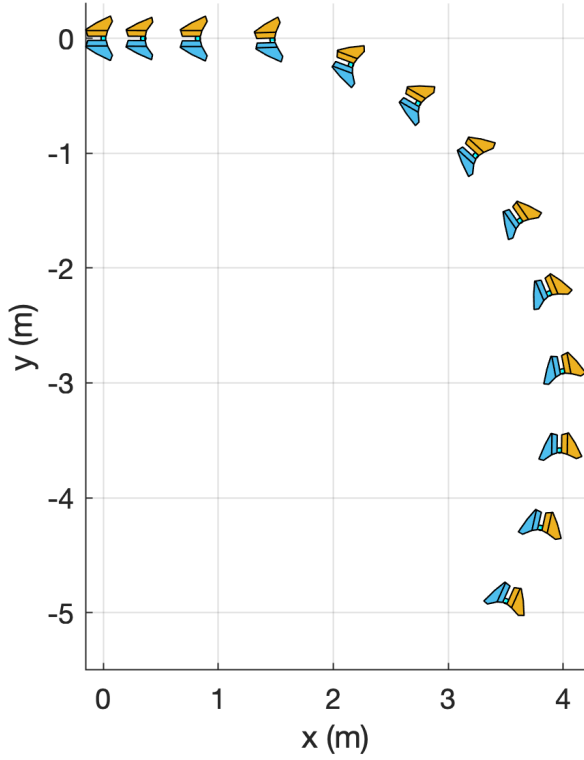


Fig. 6. Illustrates snapshots of Aerobat performing controlled 3D path tracking (banking turn) by utilizing a collocation controller to regulate its actuators.

from the computational structure at these discrete times into a single vector denoted by \mathcal{Y} and form a decision parameter vector that the optimizer finds at once. Additionally, we append the final discrete time t_f as the last entry of \mathcal{Y} so that gaitcycle time too is determined by the optimizer.

$$\mathcal{Y} = [Y_1^\top(t_1), \dots, Y_n^\top(t_n), \Omega_1^\top(t_1), \dots, \Omega_m^\top(t_n), t_f]^\top \quad (11)$$

We approximate the regulator's action at time $t_i \leq t < t_{i+1}$ as the linear interpolation function $\tilde{\Omega}(t)$ between $\Omega_i(t_i)$ and $\Omega_{i+1}(t_{i+1})$ given by

$$\tilde{\Omega}(t) = \Omega_i(t_i) + \frac{t - t_i}{t_{i+1} - t_i} (\Omega_{i+1}(t_{i+1}) - \Omega_i(t_i)) \quad (12)$$

We interpolate the computational structure states $Y_i(t_i)$ and $Y_{i+1}(t_{i+1})$ as well. However, we use a nonlinear cubic interpolation, which is continuously differentiable with $\tilde{Y}(s) = \mathbf{F}(Y(s), \Omega(s), s)$ at $s = t_i$ and $s = t_{i+1}$, where \mathbf{F} denotes the full-dynamics of Aerobat.

To obtain $\tilde{Y}(t)$, we formulate the following system of

equations:

$$\begin{aligned} \tilde{Y}(t) &= \sum_{k=0}^3 c_k^j \left(\frac{t - t_j}{h_j} \right)^k, \quad t_j \leq t < t_{j+1}, \\ c_0^j &= Y(t_j), \\ c_1^j &= h_j \mathbf{F}_j, \\ c_2^j &= -3Y(t_j) - 2h_j \mathbf{F}_j + 3Y(t_{j+1}) - h_j \mathbf{F}_{j+1}, \\ c_3^j &= 2Y(t_j) + h_j \mathbf{F}_j - 2Y(t_{j+1}) + h_j \mathbf{F}_{j+1}, \end{aligned} \quad (13)$$

where $\mathbf{F}_j := \mathbf{F}(Y(t_j), \Omega(t_j), t_j)$, $h_j := t_{j+1} - t_j$.

The interpolation function \tilde{Y} utilized for Y needs to fulfill the computational structure's derivative requirements at discrete points and at the midpoint of sample times. By examining Eq. 13, it is evident that the derivative terms at the boundaries t_i and t_{i+1} are satisfied. Hence, the only remaining constraints in the nonlinear programming problem are the collocation constraints at the midpoint of $t_i - t_{i+1}$ time intervals, the inequality constraints at t_i , and the constraints at t_1 and t_f , all of which are included in the optimization process.

Given that the computational structure is spatially discrete and incurs significant costs associated with its curse of dimensionality, this collocation scheme reduces the number of parameters for interpolation polynomials, thereby enhancing computational performance. We address this optimization problem using MATLAB's `fmincon` function.

V. RESULTS AND DISCUSSIONS

Banking turn experiments were carried out with the assistance of a Kinova robotic arm, during which force and moment measurements were captured using an ATI load cell, as detailed in Figure 2. Throughout these experiments, Aerobat- β executed flapping and banking maneuvers under varied conditions. We collected seven distinct datasets, maintaining a constant pitch angle of -15 degrees across all experiments. In four of these tests, the roll angle of Aerobat- β was set at 10, 15, 20, and 25 degrees, respectively. For the remaining three tests, while keeping the roll angle fixed at 15 degrees, we varied the Aerobat- β 's forward speed through 0.7 m/s, 0.8 m/s, and 0.9 m/s to observe the effects on banking performance.

For the banking turn simulation, Aerobat's nonlinear dynamical system was numerically solved using the fourth-order Runge-Kutta method. A collocation-based optimization controller was integrated to establish the desired roll and pitch angles. Computational efficiency was enhanced by adopting a 5-step prediction horizon. The simulation ran with a time step of 0.0001 seconds, while the controller's update frequency was set to 200 Hz, corresponding to a time step of 0.005 seconds. In the simulation parameters, Aerobat maintained a flapping rate of 3.5 Hz, matching the experimental setup. The reference pitch angle was consistently held at a negative 15 degrees, while the reference roll angle was set at 0 degrees initially for one second and then adjusted to 15 degrees for the remaining 4 seconds to execute the banking turn.

The plots in Fig. 3 provide a comparative analysis of experimental and simulated data for force and moment

measurements across 0.85 seconds, corresponding to three flapping gait cycles of the Aerobat. In the force graphs (Fx, Fy, Fz), the shaded regions represent the range of all experimental data, capturing the maximum and minimum values for each timestamp, which are depicted in red. The simulation data, shown in black, aligns closely with the average trend of the experimental data but exhibits some variations, especially in the Fx and Fy components. As for the moment graphs (Mx, My, Mz), both experimental and simulated data follow similar patterns. Both the forces (Fx, Fy, Fz) and moments (Mx, My, Mz) exhibit periodicity with similar magnitudes at the completion of each gait cycle, reflecting the robot's flapping motion. The force in the z-axis ranges from -0.5 to 0.5 N in the experimental data, suggesting the flapping-induced forces are significant, while it ranges from -0.3 N to 0.3 N in simulation. The periodic positive moment along the Y-axis for both experiments and simulation suggests that the robot experiences an upward and downward pitching motion. This behavior is anticipated, considering the tail-less design of the Aerobat.

Wake structures and vorticity around the wingtip are depicted in Fig. 4, highlighting the dynamic interactions between the Aerobat and the air during various phases of a flapping cycle. The vorticity noticeably increases during the downstroke, signaling enhanced aerodynamic forces, and reduces as the wings are folded in the upstroke, indicating a drop in aerodynamic engagement. Initially, the vorticity distribution appears symmetrical, indicative of stable flight. Yet, with the onset of banking, an asymmetrical pattern of vorticity develops, showcasing distinct disparities across the Aerobat's wings.

Figure 5 showcases the robot's dynamical states, including orientation and body angles. The pitch angle of the robot oscillates around a constant value of -15 degrees, with an amplitude ranging from 7 to 10 degrees due to the wing flapping motion. Additionally, the roll angle is precisely held at 15 degrees, enabling a significant change in the yaw angle that facilitates a smooth banking turn. Throughout the 5-second trajectory, the robot covers a distance of 4.1 meters in the x-direction and 5 meters in the y-direction. Successful 3D banking turns, achieved in both simulation and experiment, are illustrated through snapshots of Aerobat, as shown in Fig. 2 and Fig. 6.

VI. CONCLUDING REMARKS

This study has successfully enhanced the accuracy of an aerodynamic Fluid-Structure Interaction (FSI) model, enabling the controlled 3D flight path tracking of the dynamic, morphing-winged drone, Aerobat. Through experimentation and simulation, including the fine-tuning of the unsteady model for banking turn maneuvers and the integration of a collocation-based control strategy, this work has demonstrated improvements in predicting complex 3D maneuvers and achieving precise flight control.

Moving forward, future efforts will concentrate on enhancing the precision of the model, investigating how changing trajectories of flight impact Aerobat's FSI, and broadening

the drone's agility to encompass a wider range of intricate aerial maneuvers. These efforts aim to bridge the gap between theoretical models and real-world applicability.

REFERENCES

- [1] T. Y. Hubel, D. K. Riskin, S. M. Swartz, and K. S. Breuer, "Wake structure and wing kinematics: The flight of the lesser dog-faced fruit bat, *Cynopterus brachyotis*," *Journal of Experimental Biology*, vol. 213, no. 20, pp. 3427–3440, Oct. 2010.
- [2] M. Karpelson, Gu-Yeon Wei, and R. J. Wood, "A review of actuation and power electronics options for flapping-wing robotic insects," in *2008 IEEE International Conference on Robotics and Automation*, May 2008, pp. 779–786.
- [3] J.-S. Bae, T. M. Seigler, and D. J. Inman, "Aerodynamic and Static Aeroelastic Characteristics of a Variable-Span Morphing Wing," *Journal of Aircraft*, vol. 42, no. 2, pp. 528–534, Mar. 2005.
- [4] D. K. Riskin, A. Bergou, K. S. Breuer, and S. M. Swartz, "Upstroke wing flexion and the inertial cost of bat flight," *Proceedings. Biological Sciences*, vol. 279, no. 1740, pp. 2945–2950, Aug. 2012.
- [5] E. Chang, L. Y. Matloff, A. K. Stowers, and D. Lentink, "Soft biohybrid morphing wings with feathers underactuated by wrist and finger motion," *Science Robotics*, vol. 5, no. 38, Jan. 2020.
- [6] M. Di Luca, S. Mintchev, G. Heitz, F. Noca, and D. Floreano, "Bioinspired morphing wings for extended flight envelope and roll control of small drones," *Interface Focus*, vol. 7, no. 1, p. 20160092, Feb. 2017.
- [7] J. Vincent, *The flying Bat Bot can swoop and dive like the real thing*, en, Library Catalog: www.theverge.com, Feb. 2017. [Online]. Available: <https://www.theverge.com/circuitbreaker/2017/2/2/14483116/bat-bot-robot-drone-biomimicry> (visited on 08/05/2020).
- [8] J. Hoff, A. Ramezani, S.-J. Chung, and S. Hutchinson, "Optimizing the structure and movement of a robotic bat with biological kinematic synergies," *The International Journal of Robotics Research*, vol. 37, no. 10, pp. 1233–1252, Sep. 2018.
- [9] E. Sihite, P. Kelly, and A. Ramezani, "Computational Structure Design of a Bio-Inspired Armwing Mechanism," *IEEE Robotics and Automation Letters*, vol. 5, no. 4, pp. 5929–5936, Oct. 2020.
- [10] E. Sihite, P. Ghanem, A. Salagame, and A. Ramezani, "Unsteady aerodynamic modeling of Aerobat using lifting line theory and Wagner's function," in *2022 IEEE/RSJ International Conference on Intelligent Robots and Systems (IROS)*, Oct. 2022, pp. 10493–10500.
- [11] A. Ramezani, X. Shi, S.-J. Chung, and S. Hutchinson, "Lagrangian modeling and flight control of articulated-winged bat robot," in *2015 IEEE/RSJ International Conference on Intelligent Robots and Systems (IROS)*, Sep. 2015, pp. 2867–2874.
- [12] A. Ramezani, X. Shi, S.-J. Chung, and S. Hutchinson, "Bat Bot (B2), a biologically inspired flying machine," in *2016 IEEE International Conference on Robotics and Automation (ICRA)*, May 2016, pp. 3219–3226.
- [13] J. Hoff, A. Ramezani, S.-J. Chung, and S. Hutchinson, "Reducing Versatile Bat Wing Conformations to a 1-DoF Machine," in *Biomimetic and Biohybrid Systems*, ser. Lecture Notes in Computer Science, Cham: Springer International Publishing, 2017, pp. 181–192.
- [14] A. Ramezani, S. U. Ahmed, J. Hoff, S.-J. Chung, and S. Hutchinson, "Describing Robotic Bat Flight with Stable Periodic Orbits," in *Biomimetic and Biohybrid Systems*, ser. Lecture Notes in Computer Science, Cham: Springer International Publishing, 2017, pp. 394–405.
- [15] J. Hoff, A. Ramezani, S.-J. Chung, and S. Hutchinson, "Synergistic Design of a Bio-Inspired Micro Aerial Vehicle with Articulated Wings," in *Robotics: Science and Systems XII*, Robotics: Science and Systems Foundation, 2016.
- [16] E. Sihite and A. Ramezani, *Wake-Based Locomotion Gait Design for Aerobat*, arXiv:2212.05359 [cs, eess], Dec. 2022. DOI: 10.48550/arXiv.2212.05359. [Online]. Available: <http://arxiv.org/abs/2212.05359> (visited on 05/17/2023).
- [17] Y. J. Lee, K. B. Lua, T. T. Lim, and K. S. Yeo, "A quasi-steady aerodynamic model for flapping flight with improved adaptability," *Bioinspiration & Biomimetics*, vol. 11, no. 3, p. 036005, Apr. 2016.

- [18] L. Schenato, D. Campolo, and S. Sastry, "Controllability issues in flapping flight for biomimetic micro aerial vehicles (MAVs)," in *42nd IEEE International Conference on Decision and Control (IEEE Cat. No.03CH37475)*, vol. 6, Dec. 2003, 6441–6447 Vol.6.
- [19] J. Boutet and G. Dimitriadis, "Unsteady Lifting Line Theory Using the Wagner Function for the Aerodynamic and Aeroelastic Modeling of 3D Wings," *Aerospace*, vol. 5, no. 3, p. 92, Sep. 2018.
- [20] J. S. Izraelevitz, Q. Zhu, and M. S. Triantafyllou, "State-Space Adaptation of Unsteady Lifting Line Theory: Twisting/Flapping Wings of Finite Span," *AIAA Journal*, vol. 55, no. 4, pp. 1279–1294, Apr. 2017.
- [21] A. Dhole, B. Gupta, A. Salagame, *et al.*, *Hovering Control of Flapping Wings in Tandem with Multi-Rotors*, arXiv:2308.00183 [cs, eess], Jul. 2023. DOI: 10.48550/arXiv.2308.00183. [Online]. Available: <http://arxiv.org/abs/2308.00183> (visited on 10/19/2023).
- [22] E. Sihite, P. Kelly, and A. Ramezani, "Mechanism Design of a Bio-inspired Armwing Mechanism for Mimicking Bat Flapping Gait," *arXiv:2010.04702 [cs]*, Oct. 2020.
- [23] L. Landau and E. Lifshitz, *Mechanics: Volume 1*. Elsevier Science, 1982, ISBN: 9780080503479. [Online]. Available: <https://books.google.com/books?id=bE-9tUH2J2wC>.
- [24] E. Sihite, A. Salagame, P. Ghanem, and A. Ramezani, "Actuation and Flight Control of High-DOF Dynamic Morphing Wing Flight by Shifting Structure Response," in *Conference on Decision and Control (CDC)*, Singapore, Dec. 2023.